Two-well terahertz quantum cascade lasers with suppressed carrier leakage

Asaf Albo, Yuri V. Flores, Qing Hu, and John L. Reno

Citation: Appl. Phys. Lett. **111**, 111107 (2017); doi: 10.1063/1.4996567
View online: http://dx.doi.org/10.1063/1.4996567
View Table of Contents: http://aip.scitation.org/toc/apl/111/11
Published by the American Institute of Physics

Two-well terahertz quantum cascade lasers with suppressed carrier leakage

Asaf Albo,[1,2,a)] Yuri V. Flores,[1] Qing Hu,[1] and John L. Reno[3]
[1]*Department of Electrical Engineering and Computer Science and Research Laboratory of Electronics, Massachusetts Institute of Technology, Cambridge, Massachusetts 02139, USA*
[2]*Faculty of Engineering, Bar-Ilan University, Ramat Gan 5290002, Israel*
[3]*Center for Integrated Nanotechnologies, Sandia National Laboratories, MS 1303, Albuquerque, New Mexico 87185-1303, USA*

(Received 17 July 2017; accepted 29 August 2017; published online 14 September 2017)

The mechanisms that limit the temperature performance of diagonal GaAs/$Al_{0.15}GaAs_{0.85}$-based terahertz quantum cascade lasers (THz-QCLs) have been identified as thermally activated leakage of charge carriers through excited states into the continuum. THz-QCLs with energetically higher-laying excited states supported by sufficiently high barriers aim to eliminate these leakage mechanisms and lead to improved temperature performance. Although suppression of thermally activated carrier leakage was realized in a three-well THz-QCL based on a resonant-phonon scheme, no improvement in the temperature performance was reported thus far. Here, we report a major improvement in the temperature performance of a two-quantum-well direct-phonon THz-QCL structure. We show that the improved laser performance is due to the suppression of the thermally activated carrier leakage into the continuum with the increase in the injection barrier height. Moreover, we demonstrate that high-barrier two-well structures can support a clean three-level laser system at elevated temperatures, which opens the opportunity to achieve temperature performance beyond the state-of-the-art. *Published by AIP Publishing.*
[http://dx.doi.org/10.1063/1.4996567]

The maximum operating temperature (T_{max}) reported so far for a pulsed operation of terahertz quantum cascade lasers (THz-QCLs) is ~200 K.[1] For THz-QCLs based on spatially vertical transitions, the major physical mechanism that limits T_{max} was identified as thermally activated LO-phonon scattering from the upper to the lower laser level.[2] A strategy for counteracting the temperature degradation of THz-QCLs is to reduce the thermally activated LO-phonon scattering by using diagonal structures.[3]

In previous studies, we investigated potential mechanisms that limit the temperature performance of diagonal THz-QCLs and identified that thermally activated leakage of charge carriers into the continuum[4] or into excited bound states[5–7] reduces the upper laser level lifetime. Structures with widely separated higher-laying excited states enabled by using high barriers were implemented to reduce the adverse effects of these mechanisms. The suppression of those leakage channels in a resonant-phonon scheme was demonstrated[7]—as indicated by the observation of negative differential resistance (NDR) at room temperature as well as a similar current-voltage curve to those of low temperatures. However, no improvement in the temperature performance was observed.

Here, we report on a significant improvement of the temperature performance of the direct-phonon two-well (TW) THz-QCL structure by increasing the injection barrier height. Our analysis indicates that the improvement in temperature performance is due to the suppression of thermally activated carrier leakage into the continuum through the first excited resonant state. Moreover, we experimentally demonstrate that the high-barrier two-well structure can support a clean three-level laser system, that is, most of the electrons reside in the three lowest subbands even at elevated temperatures. This development opens an opportunity to achieve temperature performance beyond the state-of-the-art.

TW-THz-QCLs[8,9] have several advantages over resonant-phonon structures, which require at least three quantum wells. It has very fast depopulation of the lower laser level (LLL) solely by a LO-phonon scattering, and it is less sensitive to misalignment of the laser levels due to the Poison effect.[10] However, its reduced number of barriers also increases various carrier leakage channels, including (non-thermally activated) inter-module leakage.

In this study, we investigate a moderately diagonal ($f \sim 0.5$) two-well THz-QCL similar to that of Ref. 8 with an increased injection barrier height (device HB1, MBE wafer VA0869) and compare its temperature performance with a reference device (device LB1, MBE wafer VB0227). Device HB1 is designed to have similar parameters to device LB1 but with the injection barrier height increased by ~110–130 meV with a higher Al concentration (30%). The notations "LB" and "HB" stand for "low barriers" and "high barriers," respectively, i.e., barriers with the standard composition of 15% aluminum and with a higher composition of 30% aluminum. More details on these devices are summarized in Figs. 1(a) and 1(c), Tables I and II.

The band structure, pulsed light-current (L-I) measurements, and lasing spectra of devices HB1 and LB1 are shown in Fig. 1. As evidenced from the experimental data, T_{max} improved significantly (by ~52 K, from ~121 K to ~173 K) in the device with the increased injection barrier height. In order to understand the origin of this improvement, we analyze in-depth the measured characteristics of devices HB1 and LB1. The experimental results are presented in Figs. 1(b), 1(d), 2, and 3.

a)asafalbo@gmail.com

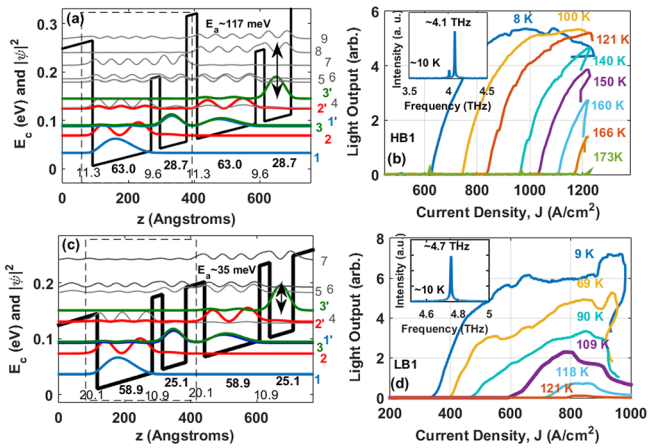

FIG. 1. (a) Band diagram of two sequential periods termed *module i* (left, marked by dashed box) and *module i + 1* (right) and (b) pulsed light–current measurements for device HB1 (VA0869) with its lasing spectra (inset). (c) Similar band diagram and (d) pulsed light–current measurements for device LB1 (VB0227) with its lasing spectra (inset). Likely excited states that are responsible for the temperature degradation are marked.

The immediate observation is the distinctive difference between the deterioration of the output power of the two devices with temperature. We analyzed the output power dependence on temperature based on the method in Ref. 2. The normalized maximum output power dependence on temperature is presented in Fig. 2(a). The output power of device LB1 starts to decrease at low temperatures around 50 K and deteriorates at a relatively moderate rate. The output intensity of device HB1 remains approximately constant up to ~130 K, but above that value, it drops sharply.

To identify the physical mechanisms underlying this behavior, we extracted the activation energies from the Arrhenius plots according to $\ln\left(1-\frac{P_{out}(T)}{P_{outmax}}\right) \approx \ln(a) - \frac{E_a}{kT}$ as performed in Ref. 2, where P_{out} is the output power and a is a constant. The experimental curves and activation energies are presented in Fig. 2(b). A clear difference is observed between devices HB1 and LB1. The activation energy of device LB1 is extracted from the high-temperature end due to the limited lasing temperature range of this device. This

TABLE I. Main design parameters and device data.

Device	Design name (wafer number)	Lasing energy [meV]	E_{21} [meV]	Oscillator strength	Expected activation energy [meV] for LO-phonon scattering	Layer sequence [#ML[a]], barrier composition, and doping level	Process details[b]
LB1	TW246 (VB0227)	20	37	0.52	16	**20.1**/25.1/**10.9**/58.9 246 periods (total thickness of ~8 μm) GaAs/**$Al_{0.15}Ga_{0.85}As$** 1.3×10^{16} cm^{-3} in the 58.9 ML well (2.2×10^{10} cm^{-2}).	MM (100 Å Ta/2500 Å Au and 100 Å Ta/3000 Å Au) Top contact n^+ layer was removed Dry Etched
HB1	TW314K-M7 (VA0869)	20	36	0.53	16	***11.3***/28.7/**9.6**/63 314 periods (total thickness of ~10 μm) GaAs/mixed barriers ***$Al_{0.3}Ga_{0.7}As$ (Inj.)*** and **$Al_{0.15}Ga_{0.85}As$ (Rad.)** 1.3×10^{16} cm^{-3} in the 63 ML well (2.3×10^{10} cm^{-2})	MM (100 Å Ta/2500 Å Au and 100 Å Ta/3000 Å Au) Top contact n^+ layer was removed Dry Etched
HB2	TW354K-M3 (VB0747)	16	55	0.18	20	**13.5**/25.5/**11.0**/50.2 354 periods (total thickness of ~10 μm) GaAs/**$Al_{0.3}Ga_{0.7}As$** 1.26×10^{17} cm^{-3} in the centered 17 ML of the 50.2 ML well (6.0×10^{10} cm^{-2})	MM (100 Å Ta/2500 Å Au and 100 Å Ta/3000 Å Au) Top contact n^+ layer was removed Dry Etched

[a]In the layer sequence column, the #ML stands for the number of monolayers, where the AlGaAs barriers in **bold** and the GaAs wells in roman, the doped layer in the sequence is underscored and the barriers' composition and doping details are elaborated in the following lines.
[b]In the process details column: the MM stands for the metal-metal waveguide, where in the following brackets are the metal sequence used for the bottom and top metallization, respectively (the metallization of the receptor n^+ layer is the same as the bottom metalization). In the lower line, the type of the etching method used in the process is mentioned.

TABLE II. Device parameters and performance.

Device	Design name (wafer number)	Injection coupling[a] ($2\hbar\Omega_{ij}$) (meV)	Design electric field (kV/cm)	τ^0_{ul} (ps)[b]	τ^0_{21} (ps)[c]	τ^0_{31} (ps)[d]	Lasing energy (meV)	J_{th}(10K) (A/cm^2)	J_{max}(10K) (A/cm^2)	Dynamic Range (10K) (A/cm^2)	T_{max} (K)
LB1	TW246 (VB0227)	1.96	17.5	1.02	0.19	4.2	20	336	981	645	121
HB1	TW314K-M7 (VA0869)	2.00	17.6	0.97	0.16	3.8	17	660	1243	583	173
HB2	TW354K-M3 (VB0747)	2.13	24.8	1.94	0.41	14.2	11	924	1106	182	134

[a]The injection coupling values correspond to our standard values for resonant phonon designs.
[b]ULL to LLL raw LO-phonon scattering time.
[c]LLL (level 2) to Injector (level 1) LO-phonon scattering time.
[d]ULL (level 3) to Injector (level 1) LO-phonon scattering time.

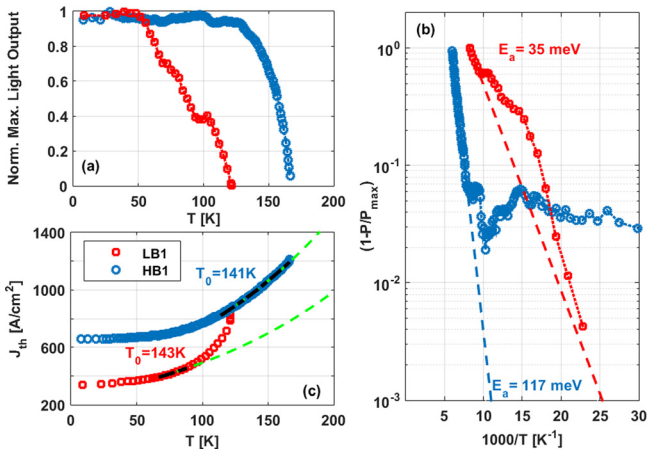

FIG. 2. (a) Normalized output light intensity versus temperature and (b) semi-logarithmic plots of $(1-\frac{P_{out}(T)}{P_{out\,max}})$ with fittings (dashed lines) and activation energy values. The reduced acuracy in the low temperature output power data of device LB1 [as being extracted from the fluctuating low temperature curves in Fig. 1(d)] is insignificant to the activation energy value, which being extracted from the high temperature side of the data. (c) Threshold current densities versus temperature with T_0 values (and data marked for extraction with extrapolation).

approach is valid based on our previous studies[2,4,7] and the consistency of the entire experimental results. The extracted activation energy value of device LB1, ~35 meV, suggests that carrier leakage into the continuum through the first excited state [level 4 of *module i* or 5 and 6 *module i + 1* in Fig. 1(c)] is likely responsible for the temperature degradation, in agreement with Ref. 4. Based on earlier studies, we exclude thermal backfilling as a major factor at temperatures below ~140 K (see, for example, Ref. 11). For the device HB1, the exponential behavior of the normalized power drop is clearly seen over a two-decade span accompanied by a significantly higher activation energy of ~117 meV, validating our approach.

The activation energy value of device LB1 suggests that thermal excitation of carriers occurs for states located energetically near the top of barriers. Such resonances undergo strong interactions with the continuum and thus have significant broadening,[12,13] which results in a very fast escape into the continuum. Consequently, once this leakage channel becomes energetically allowed at high temperatures, the deterioration will be very fast. In structure HB1, however, this leakage channel into the continuum is suppressed by the increased barrier height which reduces the interaction of this excited state with the continuum and slows down the escape rate. Accordingly, based on the above experimental results, our interpretation is that the main limiting mechanism for device HB1 is the thermally activated leakage through higher laying excited bound states located ~117 meV above the upper laser level (ULL) [levels 5–7 of *module i* or 8–9 of *module i + 1* in Fig. 1(a)].

To further verify our interpretation, we investigated the behavior of the threshold current density and the current–voltage (I–V) curves of both devices. Figure 2(c) shows the threshold current density, J_{th}, dependence on temperature. For device HB1, J_{th} rises exponentially at high temperature and its behavior can be well characterized by the standard model of $J_{th}(T) = J_o e^{T/To}$ with $T_o \approx 141$ K. For device LB1, however, the exponential behavior only occurs at temperatures not too close to T_{max}, with $T_o \approx 143$ K, whereas at temperatures near T_{max} a super-exponential rise is observed and J_{th} rises sharply. Based on our previous studies,[4] this super-exponential rise in the threshold current is a telltale sign for the onset of the leakage into the continuum, which significantly reduces the ULL lifetime at high temperatures. These results are consistent with those of Ref. 4 and support the interpretation of the relaxation mechanism based on the activation energies presented above. The increased low-temperature threshold current of device HB1 is attributed to effects of the increased injection barrier height and aluminum composition.

The I–V curves of these devices are presented in Figs. 3(a) and 3(b) at low temperature and at maximum lasing temperatures, i.e., at ~10 K and ~173 K and ~120 K for devices HB1 and LB1, respectively. The observation of an NDR behavior at the maximum operating temperature of device HB1 indicates an effective suppression of the leakage into the continuum in device HB1. Slightly above the maximum lasing temperature the NDR behavior disappears, which implies that excitation of carriers into higher lying levels limits this structure's temperature performance. In device LB1, the NDR behavior is totally wiped out even at temperatures lower than its maximum lasing temperature, which indicates that a parallel leakage channel dominates the transport, limiting the temperature performance and affecting the device characteristics already below that temperature. These findings further validate the interpretation that the limiting mechanism in device HB1 is the thermal excitation of carriers into higher lying states, and in device LB1, it is the thermal escape of carriers into the continuum through broadened excited resonance states. Furthermore, this is the first report of a performance improvement of a THz-QCL by using barriers with Al composition higher than 15%[7] and by using variable barrier heights.[14] This also indicates that the growth technique is highly accurate and well controlled.

Motivated by the significant improvement of the temperature performance, we explored whether an isolation of a three-level system (except the resonant tunneling between adjacent modules) can be achieved with the TW scheme even at room temperature; by this, we mean that electrons only occupy the lowest three bound states. For this purpose,

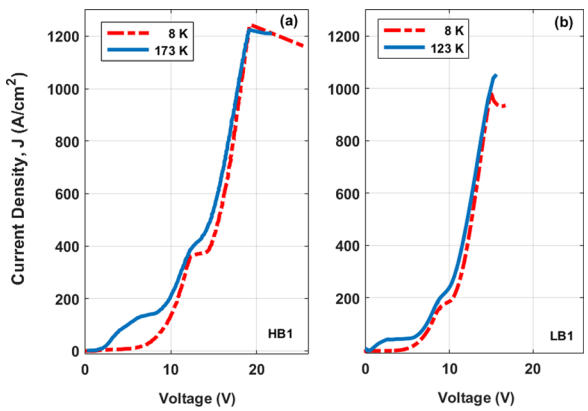

FIG. 3. Measured current–voltage curves at low temperature ~10 K (red dashed lines) and maximum operating (blue solid lines) for devices HB1 (a) and LB1 (b).

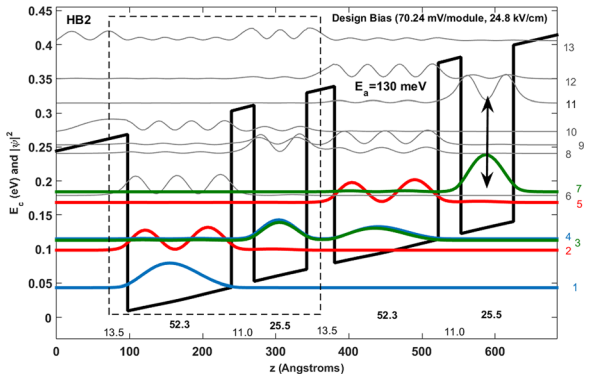

FIG. 4. Band diagram of two sequential periods for device HB2 (VB0747). The excited state that was identified in device HB1 responsible for the temperature degradation was pushed to higher energy.

we designed another high-barrier TW structure (HB2, Fig. 4, Tables I and II) with thinner wells and all barriers with 30% aluminum composition, in order to further push the excited states to higher energies. Resonant leakage channels to next module states were also minimized by the additional higher barrier. The structure was designed with a highly diagonal ($f \sim 0.18$) optical transition, and its doping was increased to compensate for the reduced gain.[15] Device HB2 demonstrates lasing with the lowest oscillator strength so far reported for THz-QCLs ($f \sim 0.18$). The previously reported lowest oscillator strength value is $f \sim 0.19$.[16]

The I–V curves of device HB2 are presented in Fig. 5(a) at low, maximum lasing, and room temperatures, i.e., ∼10 K, ∼134 K, and ∼290 K, respectively. Clear NDR behavior is observed all the way to room temperature, indicating that no significant leakage through excited states is

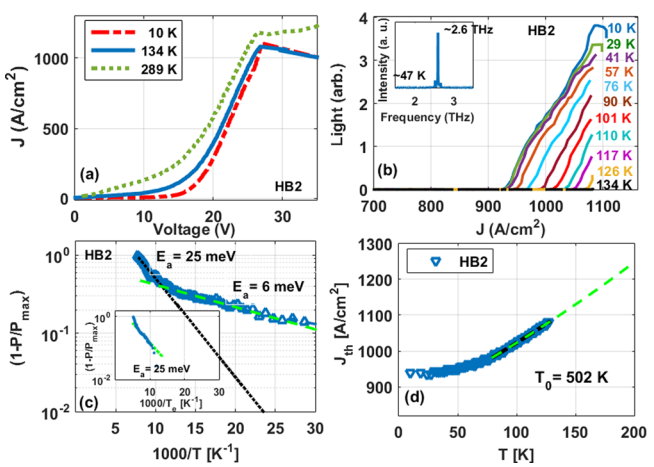

FIG. 5. Device HB2: (a) Measured current–voltage curves at low temperature ∼10 K (red dashed lines), maximum lasing (blue solid line), and room temperature (green dotted line). (b) Pulsed light–current measurements and lasing spectrum (inset) recorded at the maximum current ∼1100 A/cm^2 (right before NDR). (c) Normalized output light intensity versus temperature in semi-logarithmic plots of $(1 - \frac{P_{out}(T)}{P_{out\,max}})$ with fits (dashed lines) and activation energy values. The low-temperature data (below 100 K) demonstrate effectively lower activation energy (∼6 meV, green dashed line) due to significant excess electron temperature at that temperature range.[2] Including a characteristic excess temperature of ∼65 K in an Arrhenius plot presentation as a function of the total electron temperature rather than the lattice one results in an activation barrier of ∼25 meV for the low-temperature data (inset), similarly to the high-temperature data with zero excess electron temperature [black dotted line in Fig. 5(c)]. (d) Measured threshold current density versus heat sink temperature with T_0 value (and data marked for extraction with extrapolation).

present. Device HB2 lased at ∼2.6 THz [Fig. 5(b) inset]. The pulsed L-I measurements [Fig. 5(b)] are linear without any saturation effects which suggest an elimination of inter-module leakage channels by the increased barrier heights. For comparison, see the low temperature saturated output powers (sublinear L-I) of devices LB1 and HB1 in Figs. 1(b) and 1(d) that result from non-thermally activated inter-module leakage.[17] The experimental activation energy of device HB2 (as extracted from the high-temperature side of the data, where the electron temperature is efficiently cooled down to the lattice temperature[2]) presented at Fig. 5(c) (∼25 meV) is the expected value for thermally activated LO-phonon scattering, i.e., $E_{LO} - h\nu$. This result indicates an effective suppression of thermally activated leakage channels through excited states. The threshold current density, J_{th}, of device HB2 presented at Fig. 5(d), rises exponentially at high temperature and its behavior can be well characterized by the standard model of $J_{th}(T) = J_o e^{T/To}$ with $T_o \approx 502$ K. The increased low temperature threshold current is attributed to the higher doping and reduced oscillator strength. Altogether, the experimental results indicate that the three levels are effectively isolated from higher-lying states, the whole structure forming a clean cascaded three-level system.

Exploring further the Arrhenius plot of Fig. 5(c), we identify another activation energy at the low temperature side of the data, i.e., ∼6 meV. We speculate that this change in the slope is related to the cooling of electrons. At high temperatures, where the ULL temperature approaches the lattice temperature, we measure an activation energy value that corresponds to the ULL to LLL thermally activated LO-phonon scattering. However, the low temperature value is not the real physical activation energy simply because, at low temperatures, electrons at the ULL are much hotter than the lattice. Including a characteristic excess temperature of ∼65 K in an Arrhenius plot presentation as a function of the total electron temperature rather than the lattice one will result in an activation barrier of ∼25 meV for the low temperature data [Fig. 5(c) inset[22]], which is similar to what extracted from the high temperature data with zero excess electron temperature. We consider that the apparent smaller slope gives a strong indication for an inefficient electron cooling of the ULL at low temperatures (below ∼90 K) in TW structures. Similar reduced slope behaviour is observed for device HBD (VB0676) in Fig. 3(d) of Ref. 7, however, only at temperatures below ∼60 K, which indicates a more efficient electron cooling in three-well devices.

The limited T_{max}∼134 K of device HB2 is attributed to line-broadening, caused by the large overlap of the active states with the doping location, and to the low oscillator strength. Additional detrimental effects that are related to the thinner wells being used to push the excited states to higher energy are the slower LLL depopulation due to the off-resonance LO-phonon scattering[7] and interface roughness effects.[18] Improved temperature performance can be achieved with larger oscillator strength, as it is understood that there may be an optimized range of diagonality for high-temperature performance.[15] The thermally activated upper-to-lower state LO-phonon scattering time will be still longer than 2 ps at room temperatures even with $f \sim 0.5$, which

compares favorably to the calculated ~0.4-ps extraction time for the direct-phonon depopulation scheme of device HB2. Further improvement could be made if in addition to increasing the energy separation from the excited states one may be able to further reduce the wavefunction overlap with these states.[19–21]

Furthermore, device HB2 is a TW version of device VB0743 of Ref. 7. Comparing the temperature performance of device HB2 ($T_{max} \sim 134$ K) with a reference VB0743 device ($T_{max} \sim 151$ K)—a similar VB0743 device to that of Ref. 7 but with the equivalent fabrication process quality to that of device HB2—we identify reduced laser performance for device HB2 that is attributed to the increased overlap of the doped region with the active laser states in the TW scheme. Pushing the doped region further away from the active laser states of the TW scheme should result in additional improvement of the laser performance.

In conclusion, we have studied the temperature performance of two-well THz-QCLs with increased injection barrier height in comparison to a reference device. We have observed improved temperature performance in the high-barrier device that is attributed to the elimination of the carrier leakage into the continuum. Moreover, we have demonstrated a clean three-level system based on the two-well scheme. We further point to the direction for further improvement: increasing the active region gain through minimizing gain broadening effects and optimizing the oscillator strength value.

A. Albo would like to acknowledge the generosity of the Bar-Ilan University Engineering Faculty Fellowship as well as the MIT-Technion and Andrew and Erna Finci Viterbi Fellowships for their support during this study. Y. V. Flores would like to acknowledge the Research Fellowship Program of the German Research Foundation, DFG under Grant FL945/1–1. This work was supported by NSF, NASA, and Israel MoD. This work was also performed, in part, at the Center for Integrated Nanotechnologies, an Office of Science User Facility operated for the U.S. Department of Energy (DOE) Office of Science. Sandia National Laboratories is a multi- mission laboratory managed and operated by National Technology and Engineering Solutions of Sandia, LLC., a wholly owned subsidiary of Honeywell International, Inc., for the U.S. Department of Energy's National Nuclear Security Administration under contract DE-NA-0003525.

[1]U. S. Fathololoumi, E. Dupont, C. W. I. Chan, Z. R. Wasilewski, S. R. Laframboise, D. Ban, A. Matyas, C. Jirauschek, Q. Hu, and H. C. Liu, Opt. Express **20**(4), 3866 (2012).
[2]A. Albo and Q. Hu, Appl. Phys. Lett **106**, 131108 (2015).
[3]S. Kumar, Q. Hu, and J. L. Reno, Appl. Phys. Lett. **94**, 131105 (2009).
[4]A. Albo and Q. Hu, Appl. Phys. Lett. **107**, 241101 (2015).
[5]D. Botez, S. Kumar, J. C. Shin, L. J. Mawst, I. Vurgaftman, and J. R. Meyer, Appl. Phys. Lett. **97**, 071101 (2010).
[6]Y. V. Flores, M. P. Semtsiv, M. Elagin, G. Monastyrskyi, S. Kurlov, A. Aleksandrova, J. Kischkat, and W. T. Masselink, J. Appl. Phys. **113**, 134506 (2013).
[7]A. Albo, Q. Hu, and J. L. Reno, Appl. Phys. Lett. **109**, 081102 (2016).
[8]S. Kumar, C. W. I. Chan, Q. Hu, and J. L. Reno, Appl. Phys. Lett **95**, 141110 (2009).
[9]G. Scalari, M. I. Amanti, C. Walther, R. Terazzi, M. Beck, and J. Faist, Opt. Express **18**(8), 8043 (2010).
[10]C. W. Ivan Chan, *Towards Room-Temperature Terahertz Quantum Cascade Lasers: Directions and Design* (Massachusetts Institute of Technology, Department of Electrical Engineering and Computer Science, 2015).
[11]B. S. Williams, S. Kumar, Q. Qin, Q. Hu, and J. L. Reno, "Terahertz quantum cascade lasers with double-resonant-phonon depopulation," Appl. Phys. Lett. **88**, 261101 (2006).
[12]J. Faist, *Quantum Cascade Lasers* (Oxford University Press, Oxford, UK, Great Clarendon Street, 2013).
[13]J. Faist, C. Sirtori, F. Capasso, A. L. Hutchinson, L. Pfeiffer, and K. W. West, Opt. Lett. **21**, 985 (1996).
[14]A. Jiang, A. Matyas, K. Vijayraghavan, C. Jirauschek, Z. R. Wasilewski, and M. A. Belkin, J. Appl. Phys. **115**, 163103 (2014).
[15]C. W. I. Chan, A. Albo, Q. Hu, and J. L. Reno, Appl. Phys. Lett. **109**, 201104 (2016).
[16]C. W. I. Chan, Q. Hu, and J. L. Reno, Appl. Phys. Lett. **101**, 151108 (2012).
[17]G. P. Agrawal and N. K. Dutta, *Long-Wavelength Semiconductor Laser* (Van Nostrand Reinhold Company Inc., Canada, 1986).
[18]Y. V. Flores and A. Albo, IEEE J. Quantum Electron. **53**(3), 2300208 (2017); erratum **53**(5) (published online, 2017).
[19]C.-C. Chang, *Step-Tapered Active-Region Mid-Infrared Quantum Cascade Lasers and Novel Fabrication Processes for Buried Heterostructures* (University of Wisconsin-Madison, Department of Electrical and Computer Engineering, 2015).
[20]A. Albo and Y. V. Flores, IEEE J. Quantum Electron. **53**(1), 2300105 (2017).
[21]A. Albo and Y. V. Flores, IEEE J. Quantum Electron. **53**(5), 8500508 (2017).
[22]However not likely (since we know there is efficient cooling of excess electron temperature above ~100 K in THz-QCLs[2]), if we assume that the same excess temperature holds for the high temperature side of the data it will result in activation energy of ~63 meV instead of ~25 meV (not shown in the graph) and will point to an alternative limiting mechanism, which is scattering from the ULL to the first excited state: level 6 in *module i* (and levels 8–9 in *module i + 1*) in Fig. 4 that shunts the current and limits the temperature performance.